Chromium Aromatic Hydrocarbon Sandwich Molecules and the Eighteen-Electron Rule†

Michael R. Philpott*,‡,§ and Yoshiyuki Kawazoe‡

Institute for Materials Research, Tohoku University, 2-1-1 Katahira, Sendai 980-8577, Japan

Received: August 4, 2007; In Final Form: September 25, 2007

Ab initio density functional theory (DFT) calculations are reported for the chromium sandwich structure Cr_nR_2, where $n = 7$ and R is the aromatic hydrocarbon hexabenzocoronene ($C_{42}H_{18}$). This system is remarkable in that the structure of the chromium sites strongly resemble those in chromium bis-benzene $Cr_1(C_6H_6)_2$, as judged by geometry and charge density properties. The electron localization function of the sandwich shows a hexagonally arrayed set of V(C, Cr, C) valence basins about each chromium atom with modification due to local site symmetry. This system satisfies an extension of the 18-electron rule to components of a conjugated molecular system. This idea is explored further by examining the electronic and geometric properties of the series Cr_nR_2, where n and R are given by $n = 1$, benzene C_6H_6 as reference; $n = 2$, biphenyl $(C_6H_5)_2$; $n = 3$, triphenylene $C_{18}H_{12}$; $n = 3$, coronene $C_{24}H_{18}$; and $n = 4$, dibenzopyrene $C_{24}H_{14}$. On the basis of electron counting and ring isolation, all the sandwich structures in this series could satisfy the extension of the 18-electron rule, with the exception of coronene, which was deliberately included. The DFT calculations predict spin-paired ground states for some but not all of the sandwich structures, implying that the Cr−ring interactions at work require understanding at a deeper level. Thus, while sandwiches with $n = 1$, $n = 2$, $n = 4$ and $n = 7$ have spin paired singlet ground states and appear to satisfy the rule, those with $n = 3$ (triphenylene, coronene) have antiferromagnetic singlet ground states and do not. This is attributed to nonuniformity in the electronic charge density of the rings of the isolated hydrocarbons and to a reduction of symmetry from D_{3h} to C_{2v} with a concomitant spin−charge density change in the sandwiches.

1. Introduction

In this paper, we calculate, using ab initio plane-wave-based density functional theory (DFT), the electronic and geometrical properties of selected chromium sandwich structures, Cr_nR_2, where R is a planar polycyclic aromatic hydrocarbon. This work is motivated by the recent synthetic work of Murahashi et al.[1] on palladium ($n = 3, 5$) organometallic sandwich complexes of tetracene and heptacene and subsequent studies of hypothetical sandwich structures consisting of larger aromatic hydrocarbons and transition metals, some of which support magnetism.[2−4]

In the current study, preliminary calculations of the sandwich $Cr_7(C_{42}H_{18})_2$ showed that the geometric structure around each metal atom strongly resembled that of the much smaller system chromium bis-benzene $Cr_1(C_6H_6)_2$. Both systems had singlet ground electronic states and metal−aromatic ring spacing around 162 pm. For both systems, there were similarities in the isometric surfaces of the total electric charge density and the electron localization function (ELF), implicating the operation of the 6*n* and 18e rule for these fully benzoidal hyrocarbons.[5−6]

Subsequently, a series of sandwich structures were selected on the basis of the 6*n* and 18e rules to test whether the hydrocarbon layers would be drawn together, creating the high field conditions necessary for a singlet ground state. Lest the idea be thought too simple, we included the coronene system $Cr_3(C_{24}H_{18})_2$. In this $n = 3$ structure, there were more π-electrons than needed to formally satisfy the 18e rule. Even though the number of π-electrons corresponds to $n = 4$, coronene is not a fully benzenoid hydrocarbon. These extra electrons can assist electronic coupling among the rings, which are not as electronically independent as in true fully benzenoid hydrocarbons, such as biphenyl or the molecule hexabenzocoronene.

Figure 1 shows the hydrocarbons considered in this paper using the chemical notation that denotes an aromatic sextet[7] by a circle. In passing, we note that all these hydrocarbons are physically stable, colorless or yellow materials, having electronic singlet absorption bands starting around ≥3 eV and phosphorescence emissions in the visible spectrum.[8] These are not exotic materials; for example, soluble derivatives of hexabenzocoronene have been used to make nanotube structures by self-assembly techniques.[9]

The use of circle notation here is not the same as used in organic chemistry to describe extended aromaticity. In this latter case, naphthalene would be depicted as having a circle in each ring.

In the present case, each circle corresponds to the two valence bond (VB) or "Kekulé" diagrams describing electron pairing in the C_6 ring. In this representation, coronene, as depicted in Figure 1, is an exception because there is another "equivalent" structure given by an in-plane 60° rotation of the molecule that shares the total set of VB structures. With this one exception, the hydrocarbons were selected on the basis that (i) they belonged to the fully benzenoid hydrocarbon category having $6n$ π-electrons per molecule[5] and (ii) by electron counting, they satisfied the "18-electron rule"[6] separately for each benzenoid center.

In this valence bond (VB) picture, the hydrocarbons have a ground state consisting of "weakly" coupled aromatic rings. Molecules with n "independent" C_6 rings have 2^n valence bond diagrams, where n is the number of benzenoid rings. There are

† Part of the "William A. Lester, Jr., Festschrift".
‡ Tohoku University.
§ Current address: 1631 Castro Street, San Francisco, California 94114.

10.1021/jp076251c CCC: $40.75 © 2008 American Chemical Society
Published on Web 01/23/2008

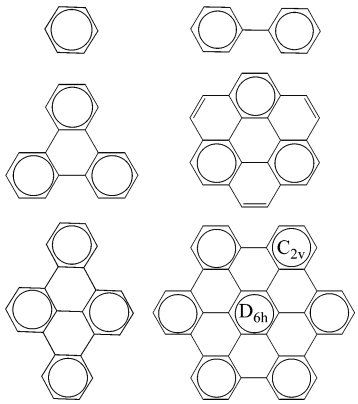

Figure 1. Schematic diagram of the hydrocarbon components of the chromium sandwich structures Cr_nR_2. In rows from left to right: benzene C_6H_6, biphenyl $C_{12}H_{10}$, *s*-triphenylene $C_{18}H_{12}$, coronene $C_{24}H_{12}$, dibenzopyrene $C_{24}H_{14}$, and *s*-hexabenzocoronene $C_{42}H_{18}$ shown with site symmetry labels.

also a few diagrams corresponding to alternating single and double bonds around the perimeter that do not belong to the benzoidal set. In the case of the molecule *s*-hexabenzocoronene ($C_{42}H_{18}$), its seven aromatic centers provide 128 (2^7) of the ($2^7 + 2$) valence bond diagrams that belong to the ground state. For the other molecules, benzene has 2 (2^1), biphenyl $(C_6H_5)_2$ has 4 (2^2), *s*-triphenylene $(C_6H_4)_3$ has 9 ($2^3 + 1$), coronene $C_{24}H_{12}$ has 10 ($2^3 + 2$), and dibenzopyrene $C_{24}H_{14}$ has 18 ($2^4 + 2$) valence bond structures.

The 18e rule correlates additional energetic or reaction stability in organometallic complexes. There are numerous papers discussing the 18e rule[10] and the sext rule,[11] and a detailed discussion is not in the scope of this paper, except to say that the effect is understood largely as due to the complete utilization of the phase space available to electrons in closed shells for a given principle quantum number. It works best for some first row transition metals. Some notable examples of the organometallic complexes satisfying the 18e rule are ferrocene $Fe_1(C_5H_5)_2$,[12] recently synthesized dizincocene $Zn_2[C_5(CH_3)_5]_2$,[13−17] and $[Cr(C_5H_5)(CO)_3]_2$.[18] For chromium and aromatic C_6 rings the 18-electron rule as considered in this report takes the very symmetric form (6 + 6 + 6).

This report is organized as follows. In the next section, we briefly describe the computational methodology. Then in separate sections, we present the results of DFT calculations with relevant comments for the sandwiches in the following order:

(1) reference molecule $Cr_1(C_6H_6)_2$ with results relevant for the rest of the paper,

(2) sandwiches for which the 18e rule held: $Cr_2[(C_6H_5)_2]_2$, $Cr_4(C_{24}H_{14})_2$, $Cr_7(C_{42}H_{18})_2$, and

(3) sandwiches $Cr_3(C_{18}H_{12})_2$ and $Cr_3(C_{24}H_{12})_2$, for which the rule did not hold.

All $n = 1$, 2, 4, and 7 sandwiches had similar chromium site geometries and unpolarized singlet ground states. In contrast, the $n = 3$ sandwiches (nominal D_{3h} geometry) containing triphenylene and coronene, formed metal−carbon bonds, and had larger Cr−ring distances consistent with their antiferromagnetic singlet ground states. The explanation of these deviations, given in the appropriate Results section, was traced to a charge distribution that deviated from the uniformity of the benzoidal ring either in the isolated hydrocarbon or in the chromium sandwich structure. Finally, the last section provides a brief summary and discussion of bonding motifs revealed by these investigations, together with a few suggestions for future study.

We use the Figures to display the overall sandwich geometry and summarize key aspects of bond distances in the text in an attempt to avoid unnecessary numerical detail.

2. Computational Methodology

All calculations were performed using the ab initio simulation package Vasp.[19−22] The plane wave calculations used the projector augmented wave (PAW) pseudopotentials[23−24] in which the nonvalence electrons are treated as a frozen core and the spin-polarized generalized gradient approximation for the exchange-correlation energy functional PW91 parametrized by Perdew and co-workers.[25−26] The advantage of plane wave methodology lies in the simplicity of the representation; improvements in accuracy are achieved by increasing the plane wave cutoff energy and the size of the simulation box. A disadvantage is the enormous size of the basis.

The use of a single determinant, as done here, to represent the spin properties of open shell systems has been widely investigated in recent years.[27−28] Our interest in this study was energy, geometry, and basic electronic structure and not in pursuing a refined study of spin and magnet properties, as done in the area of molecular magnetism. The valence electrons were assigned as follows: Cr (6), C (4), and H (1). All calculations were performed using periodic boundaries with a cubic cell and edge lengths in the range 0.75−2.50 nm so that atoms belonging to different molecules were at least 1.0 nm apart. All the Brillouin zone integrations were done at the gamma point. The geometry optimizations were carried out using the conjugate gradient method, usually until the forces acting on each atom were approximately ≤ 8 μeV/pm (0.06 cm^{-1}/pm).

During this study, we routinely calculated geometry, total energy for the given total spin, isometric surfaces of total charge and Kohn−Sham partial charges, spin density, and the electron localization function ELF.[29−30] The definition of the ELF used in this paper is the same as Becke and Edgecombe:[29]

$$\mathrm{ELF}(\mathbf{r}) = \{1 + [D(\mathbf{r})/D_h]\}^{-1} \quad (1)$$

$$D(\mathbf{r}) = \frac{1}{2}\sum_i |\nabla \varphi_i(\mathbf{r})|^2 - \frac{1}{8}|\nabla \rho(\mathbf{r})|^2/\rho(\mathbf{r}) \quad (2)$$

$$D_h = (3/10)(3\pi^2)^{5/3}(\rho)^{5/3} \quad (3)$$

Here $\{\varphi_i(\mathbf{r})\}$ ($i = 1, ..., N$) is a set of KS orbitals making up a single determinant wavefunction, $\rho_i(\mathbf{r})$ is the partial charge density assigned to the ith KS level, and $\rho(\mathbf{r}) = \sum_i \rho_i(\mathbf{r})$ is the total electron density. Electron localization occurs if the ELF value elf is >0.5, delocalization if elf is <0.5. There are no atomic core attractors in these valence electron, only simulations. The C−C bonds in organics may have one-point, two-point (M^1, M^2),[31−32] or ring attractors determined by the symmetry properties of the electron density function in the vicinity of the bond. Other features that appear in the ELF of chromium bis-benzene are nonbonding basins of d_{z2}-chromium electrons and six small hexagonally arranged basins in the plane through the metal atom parallel to the rings. The latter, described by Frison and Servin[32] in their comparison of $Fe_1(C_5H_5)_2$ and $Cr_1(C_6H_6)_2$, occur in our calculations as a bridge between the hydrocarbon valence basins.

Harmonic analysis of the wave function inside spheres with centers on individual atoms also assisted the analysis of charge density of the chemical bonds. The starting geometries were aromatic hydrocarbons with standard bond lengths. In the sandwiches, the hydrocarbons were eclipsed, and metal atoms were initially located in the middle above the ring centers. The

total energy, E_t, calculated by Vasp was also referenced to the sum of separated metal atoms and separated planar hydrocarbon molecules as ΔE_f, where

$$\Delta E_f = -\{E_{tot}[Cr_n(R)_2] - 2E_{tot}(R) - nE_{atom}(Cr)\} \quad (4)$$

In the calculations, the following conditions held: All systems were electrically neutral; all calculations were performed with unrestricted spin; the symmetry of the sandwich structures was constrained to D_{2h} or C_{2v} symmetry unless otherwise stated; and all energies were in electron volts, all distances are in picometers unless otherwise specified. In D_{2h} symmetry, the hydrocarbon layers were eclipsed and the metal atoms are restrained to the starting plane. The impact of the lower symmetry on the D_{6h} symmetric chromium bis-benzene molecule was observed to be negligible in energy and geometry because of the large binding energy and the relatively large size of the periodic box.

Visualization used the free software Vaspview and Rasmol.[33] All the plots are orthographic, without perspective. The use of a color scale to visualize and interpret density features turned out to be extraordinarily useful for interpreting chemical bonding. In the linear scale, the data is mapped into the range 0−1 and a color (blue = 0, red = 1) was assigned to each value in this range. For the logarithmic scale, the data is first scaled linearly into the range 1 to e^2 and then the natural log of the resulting value is taken and divided by 2 to provide a number between 0 and 1, which is then assigned a color. Both scales are used according to which best highlights the detail. Since electric charge densities vary enormously, in the text we quote values d_{max} ($d_{max} = 1$ for ELF) and d_{iso}, which are the value of the maximum charge and the value of the isometric surface charge, respectively.

The DFT total energies, calculated with PAW potentials, for isolated hydrocarbon molecules ($S = 0$, ground state) and Cr metal atom were as follows: benzene $E_{tot}(C_6H_6) = -76.238$ eV; D_{2h} biphenyl $E_{tot}(C_{12}H_{10}) = -145.176$ eV; triphenylene $E_{tot}(C_{18}H_{12}) = -207.305$ eV; coronene $E_{tot}(C_{24}H_{12}) = -262.980$ eV; dibenzopyrene $E_{tot}(C_{24}H_{14}) = -269.438$ eV; hexabenzocoronene $E_{tot}(C_{42}H_{18}) = -449.060$ eV; Cr atom ($S = 2$, configuration d^5s^1), $E_{atom}(Cr) = -5.445$ eV. For an isolated benzene molecule, the calculated bond distances were C−C = 140 pm and C−H = 109 pm.

In the Tables and in the text, we use the following notation to simplify entries and descriptions: M−ring, the distance from metal atom Cr to the plane of the nearest ring; Cr−C, metal−carbon distance; C−C, ring carbon bond length; C−H, carbon-hydrogen bond distance; C−C′ (or H−H′), the distance between C(H) atoms on opposing eclipsed rings. In some cases, we can approximate M−ring by half the average value of C−C′, but we never use H−H′ this way, since it is almost always significantly smaller. Where no confusion was possible, the metal atoms were sometimes referred to or labeled as M1, M2, M3, ... The coordinate axes of the sandwich were sometimes described in L (long), M (medium), or N (normal) notation.

3. Results for Chromium Bis-benzene, $Cr_1(C_6H_6)_2$

Table 1 lists the calculated geometry for the benzene sandwich alongside the geometry of the biphenyl, dibenzopyrene, and hexabenzocoronene sandwiches, which also comply with the 18e rule. The calculated DFT energies for $Cr_1(C_6H_6)_2$ were $E_{tot} = -161.147$ eV and $\Delta E_f = 3.226$ eV. The HOMO−LUMO band gap $BG_0 = 1.954$ eV. Overall, in the $Cr_1(C_6H_6)_2$ molecule, the calculated metal and carbon geometry was in good agreement with the electron diffraction[34−35] result. We also note that the calculated inter-ring H−H′ distance is smaller than the C−C′ distance. The out-of-plane tilt of the C−H bonds relative to the C6 ring is ∼3°. In the bis-benzenes of iron and palladium (not described here), the tilt was found to be very small.[36]

In Table 1, the metal−ring spacing, M−ring, was taken to be one-half the C−C′ spacing, where C and C′ are an eclipsed pair of carbon atoms on opposing rings. The entry H−H′ gives the separation of any pair of eclipsed H atoms. This distance is notably smaller than the C−C′ spacing. Half the inter-plane spacing in graphite is $^1/_2c = 167.35$pm, which is almost 4% larger than the eclipsed ring−ring spacing in chromium bis-benzene. The shortness of the interplane spacing in chromium bis-benzene and the lengthening of the C−C-ring bond provided evidence of the large extent of involvement of the metal in its bonding interaction with benzene and by inference with independent benzenoid C_6 rings. Rayon and Frenking[37] have analyzed this interaction further using the method of energy partitioning of the bond energy. Entries for other sandwiches in Table 1 show that the short metal ring distance occurs consistently in the bis-biphenyl, bis-dibenzopyrene, and bis-hexabenzocoronene structures, in accordance with the 18e rule.

The ground state of chromium bis-benzene is a singlet $S = 0$, corresponding to a small metal ring spacing gap and concomitant high field. The HOMO−LUMO gap is $BG_0 = 1.952$ eV. Harmonic analysis of the wavefunction inside a sphere around chromium radius 100 pm showed the five highest homos to be grouped in almost degenerate pairs of 3d-like functions. For all the chromium levels, explicit calculation of partial charge distributions verified the harmonic analysis, the nature of the bonding, and the ELF basin to which it contributed. All had overlap to the hydrocarbon p_π-functions except the highest homo-1 (KS-33). This level was a d_{z2}-type function that overlapped only H atom functions and not any one C atom. It contributed the nonbonding valence basin V(Cr) (see Table 2 and Figures 2 and 3). Some of the properties of the highest homos (KS levels 33−27) and the two lowest LUMO KS levels are listed in Table 2. The notation used is self-explanatory; the labels C and M (≡Cr) were added where some distinction was needed.

The isometric surfaces of the total charge showed the C−C bonds of the aromatic rings to be equivalent. If one carefully examines the topographical shape of the surfaces in the Cr−ring region, one observes hints of hexagonal cross section at higher isometric values in the column of charge surrounding the metal atom joining it to the benzene rings.

Rayon and Fenking[37] characterized the metal−carbon bond in $Cr_1(C_6H_6)_2$ as a δ-bond, as compared to π-bonding in ferrocene $Fe_1(C_5H_5)_2$. The ELF can provide a more detailed picture of the bonding than total charge. Figures 2 and 3 show some of the most important aspects of the ELF listed below. Figure 2A shows a plane slice through the ELF function that cuts through two C atoms in a para position. Superimposed is the atomic frame work (C, green; H, red). Labels V(Cr), V(C, H), V(C, Cr, C), and V(Cr, C, C) identify the four valence basins described further below. The basin V(Cr, C, C), a difficult to visualize feature close to the ring C atoms, is also identified in Figure 2B on an ELF slice through the C atoms of the aromatic ring. Three valence basins are labels. These results are in some ways different from the work of Frison and Servin,[32] who considered ELF of all electrons, not just the valence electrons, as in the present report.

We describe the ELF of $Cr_1(C_6H_6)_2$ in enough detail to be useful for interpreting the results of the sandwich structures

TABLE 1: Geometry (Distances/pm; Angles/deg) of Molecules Cr_nR_2 for R = C_6H_6, $C_{12}H_{10}$, $C_{24}H_{14}$, $C_{42}H_{18}$[a]

Benzene/$Cr_1(C_6H_6)_2/S = 0$

metal charge 6.05

Cr−ring	M−C	C−C	C−C′	H−H′	∠C1−M−C2
161/161[b]	214/215[b]	142/142[b]	322	311	38.7

Biphenyl/$Cr_2[(C_6H_5)_2]_2/S = 0$

M−M distance: Cr1−Cr2 = 442
C−C bond connecting rings: C−C = 150

Cr1 site/C_{2v} symmetry/charge 6.04

Cr1−ring	M−C	C−C	C−C′	H−H′	∠C1−M−C2
161	214	141−143	322	311	38.7

Dibenzopyrene/$Cr_4(C_{24}H_{14})_2/S = 0$

M−M distance(s): Cr1−Cr1′ (||M) = 439; Cr1−Cr2 = 438; Cr2−Cr2′ = 760
C−C bonds connecting rings: Ring1−Ring2 = 149; Ring1−Ring1′ = 148

Cr1 site/C_{2v} symmetry/charge 6.01

M1−ring	M1−C	C−C	C−C′	H−H′	∠C1−M−C2
162	Av 215	Av 142	Av 323	318	Av 38.6

Cr2 site/C_{2v} symmetry/charge 6.03

M2−ring	M2−C	C−C	C−C′	H−H′	∠C1−M−C2
Av 161	Av 215	Av 142	Av 322	314	38.6

Hexabenzocoronene/$Cr_7(C_{42}H_{18})_2/S = 0$

M−M distance(s): all nearest neighbor Cr(*i*)−Cr(*j*) = 436
C−C bonds connecting rings: radial C−C = Av 147; circumferal C−C = Av 148

Cr1 site/D_{6h} symmetry/charge 5.98

Cr1−ring	M1−C	C−C	C−C′	H−H′	∠C1−M−C2
162	216	Av 144	324	na	Av 38.8

Cr2 site/C_{2v} symmetry/charge 6.01

Cr2−ring	M2−C	C−C	C−C′	H−H′	∠C1−M−C2
162	Rg 214−216	Rg 142−144	324	316	38.6

[a] Av = average. Rg = range. C(H)−C′(H′) are eclipsed pairs of atoms in opposing hydrocarbons. [b] Haaland electron diffraction.[34,35]

TABLE 2: Kohn−Sham Energy Levels for Chromium Bisbenzene $Cr_1(C_6H_6)_2$

KS level	*E*/eV	occn	harmonic	comment	ELF basin[a]
35	−0.7859	0	Cpz	LUMO2	
34	−0.7860	0	Cpz	LUMO1	
33	−2.7384	2	dz2	nonbonding	V(M)
32	−3.9929	2	d*xy*Cpz	pπ-dπ-pπ	V(CMC)
31	−3.9935	2	d*x*2Cpz	pπ-dπ-pπ	V(CMC)
30	−6.7101	2	d*yz*Cpz	dπ-pπ	V(MCC)
29	−6.7108	2	d*xz*Cpz	dπ-pπ	V(MCC)
28	−6.9219	2	Mp*y*Cpz		
27	−6.9225	2	Mp*x*Cpz		

[a] M ≡ Cr.

formed from hexabenzocoronene, biphenyl and dibenzopyrene. Starting at ELF values (elf) near unity, the appearance and change in the various ELF features was found as follows:

(1) V(C, H) individual C−H bond valence basins appear near elf = 0.998.

(2) V(C, C) individual C−C bond basins appear near elf = 0.850.

(3) At about elf = 0.503, six small pointlike structures appear, which at elf = 0.500 have grown and linked all the V(C, C) basins, but only on the side facing the metal atom. We refer to the merged set as V(Cr, C, C). The location of these features correlates with partial charge in the degenerate levels KS-29 and -30, which are d_{zx} and d_{yz} functions.

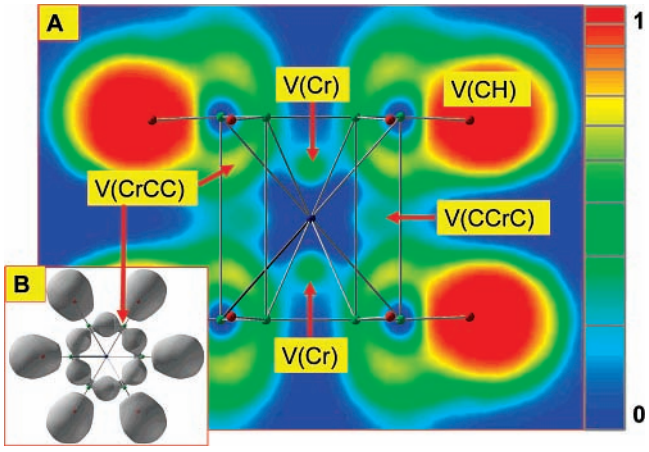

Figure 2. ELF of the molecule $Cr_1(C_6H_6)_2$ plotted on a log colored scale on a plane containing the *z*-axis and perpendicular to the benzene rings. The plane cuts through two C−H bonds on each ring. The labels identify the location of the basins V(C, H), V(Cr, C, C), V(Cr), and V(C, Cr, C). The wire bonds connect the central chromium to all C atoms, and all C atoms are connected vertically to their eclipsed counterparts. Inset panel B shows the ELF isosurface at elf = 0.500 viewed down the *z*-axis. The V(C, C) bond basins are shown linked together like a circular pearl necklace to form the V(Cr, C, C) basin.

(4) At about elf = 0.250, two V(Cr) isolated, nonbonding attractors appear on the configuration axis ~81pm from the Cr atom. These basins do not merge with other basins while ELF

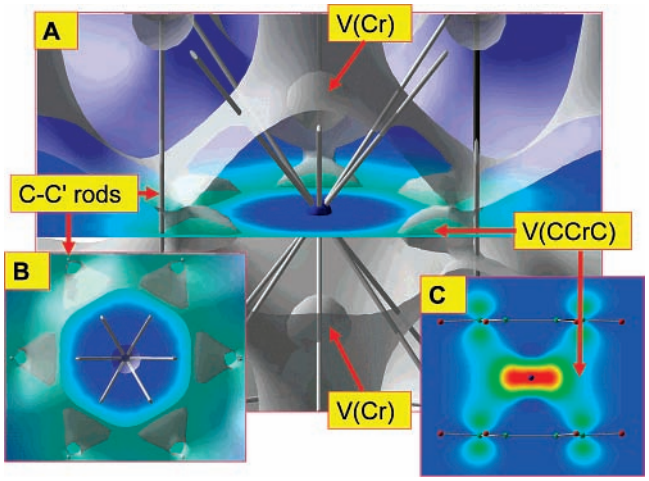

Figure 3. Detail of the ELF isosurface (elf = 0.130) of $Cr_1(C_6H_6)_2$ in the vicinity of the chromium atom. The slice plane is through the metal atom parallel to the benzene rings. Colors on the slice plane are ELF values on a log scale. The atom−atom connecting rods are the same as shown in Figure 2A. The nonbonding basin V(Cr) is visible as a rough sphere above and below the central metal. The V(C, Cr, C) shows the position of one of the hexagonal basins (the nearest basin is cut off by the viewing plane) that have merged with the hydrocarbon basins V(Cr, C, C). The inset 2B shows a plan view down the *z*-axis at a very small tilt to display the vertical C−C′ rods, which just miss where the hexagonal basins merge (light blue) with V(Cr, C, C). The rods radiating from the central atom are the six Cr−C connectors seen in panel A and in Figure 2A. Inset panel C, color log scale plot of the partial charge density of the KS-31 level showing the d_{x2-y2} function on the Cr atom overlapping carbon p_z-functions. The partial d_{x2-y2} and d_{xy} densities contribute the V(C, Cr, C) basins.

is greater than about elf = 0.08. The basins are due to the isolated d_{z2} function of the level KS-33.

(5) At elf = 0.148, a set of basins V(C, Cr, C) appears as a hexagonal array of points on the plane through the Cr atom and parallel to the rings. The attractors first appear ~102 pm from the Cr atom. At elf = 0.135, they merge with the expanding V(Cr, C, C) isosurface. At elf = 0.125, the six basins form a ring with the columns connecting the V(Cr, C, C) surfaces intact. At smaller ELF values, the six columns merge into a single stalk.

Figure 2A shows the ELF of $Cr_1(C_6H_6)_2$ on a log scale, colored plane slice containing the *z*-axis and perpendicular to the benzene rings. It shows the location of the V(C, H), V(Cr, C, C), V(Cr), and V(C, Cr, C) basins. The wire bonds connect chromium to all C atoms, and all C atoms are connected vertically to their eclipsed counterpart. Inset panel B shows the ELF isosurface for elf = 0.500 viewed along the configuration *z*-axis. The V(C, C) bond basins are shown linked together to form the V(Cr, C, C) surface. In isolated benzene, one does not observe one-sided connecting of bond basins following the appearance of the linkers.

Figure 3A shows a detail of the ELF isosurface of $Cr_1(C_6H_6)_2$ in the vicinity of the chromium atom at elf = 0.130. The slice plane is through the metal atom parallel to the benzene rings. The atom−atom "wire" bond connections are the same as in Figure 2A. The nonbonding basin V(Cr) is visible a sphere above and below the central metal atom. The label V(C, Cr, C) shows the position of one of the hexagonal basins after it has merged with the hydrocarbon basins, V(Cr, C, C). The inset panel B shows a plan view down the *z*-axis at a very small tilt in order to display the vertical C−C′ lines that just miss where the basins merge (bright blue) with V(Cr, C, C) on each side of the slicing plane. This inset shows that the "delta" bond involves

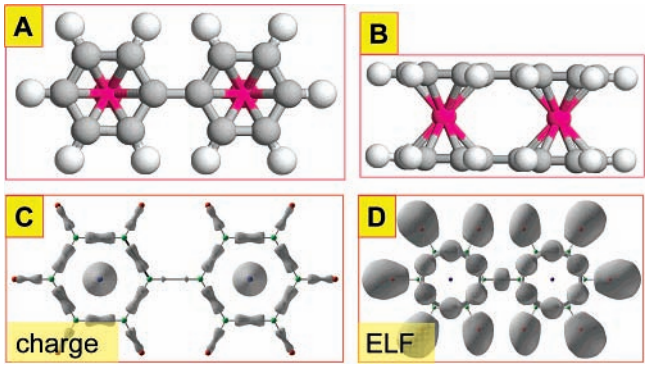

Figure 4. Geometry, electronic structure, and ELF of the biphenyl sandwich $Cr_2[(C_6H_5)_2]_2$. Panels A and B show the overall shape of the molecule as flat with the metal atoms close to the center between the rings. Panel C shows a top view of the total charge density (d_{iso} = $8500/d_{max}$ = 16 836). The bond joining the rings is weakly conjugated. Panel D is the ELF isosurface (elf = 0.491) viewed from the top. Each ring has the appearance of a circle pearl necklace (C−C bond basins) linked together on the metal side, as in chromium bis-benzene.

the d_{xy} and d_{x2-y2} degenerate pair KS-31 and KS-32 listed in Table 2. Inset panel C shows a color log scale plot of the partial charge density of the KS-31 level. This Kohn−Sham level consists primarily of a d_{x2-y2} function on the Cr atom overlapping p_z functions on the carbon atoms. Together with KS-32, the partial d_{x2-y2} and d_{xy} densities from chromium contribute the V(C, Cr, C) basins. This interpretation is aligned with the δ-bonding description of Rayon and Fenking,[37] rather than Frison and Servin,[32] who assigned these basins as nonbonding. It is the tightness of the Cr−ring gap that makes possible the δ-bonding and the concomitant spin pairing of the metal electrons.

4. Results for Biphenyl Sandwich $Cr_2[(C_6H_5)_2]_2$

The total DFT energy was calculated spin-unrestricted using a D_{2h} molecular geometry with the two rings of biphenyl lying in the same plane, not twisted (symmetry D_2), as for the molecule in the gas phase. The ground state was found to be a spin-paired $S = 0$ singlet; the DFT energy, $E_{tot}\{Cr_2[(C_6H_5)_2]_2]\}$ = −307.424 eV; and the HOMO−LUMO gap, BG_0 = 0.956 eV. The formation energy relative to separated components, ΔE_f = 6.18 eV or 3.09 eV/Cr atom, was a little less than twice the formation energy of chromium bis-benzene (ΔE_f = 3.226 eV). A search was made for an antiferromagnetic ground state in D_{2h} physical geometry but none was found. The basic geometry of the sandwich is given in Table 1, wherein a comparison with the other three 18e-compliant hydrocarbons shows a close similarity. The two rings in the biphenyl moiety were separated by C−C = 150 pm, close enough to a single C−C bond to correspond to weak conjugation between the rings. In the isolated D_{2h} biphenyl molecule, the same bond was slightly shorter, and the ELF of biphenyl had a well-defined point attractor indicative of a σ-bond without a substantial π-component.

Figure 4, panels A and B, show the overall shape of the sandwich molecule. It is flat with the metal atoms close to the center of each ring. The torsion angle between the C−H bonds and the ring plane was found to be smaller than in chromium bis-benzene. Figure 4C shows a top view of the total charge density for d_{iso} = $8500/d_{max}$ = 16 836. Each bond in the rings has a similar charge density. The central bond at this isometric value indicates a much smaller charge density.

For the most part, the ELF of the biphenyl sandwich resembled a "double-up" version of $Cr_1(C_6H_6)_2$. Figure 6D

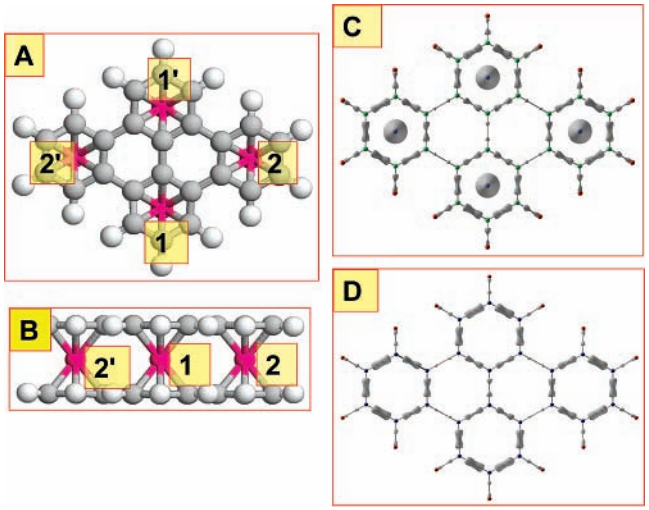

Figure 5. Geometry and electronic structure of the dibenzopyrene sandwich $Cr_{24}[(C_{24}H_{14})_2]_2$. Panels A and B show the overall shape of the molecule as flat with the metal atoms very close to the center between the rings. Panel C shows a top view of the total charge density isosurface ($d_{iso} = 14\,500/d_{max} = 28\,339$). Panel D shows the total charge density isosurface ($d_{iso} = 15\,000/d_{max} = 16\,809$) of an isolated dibenzopyrene molecule. Note the similarities in the hydrocarbon charge.

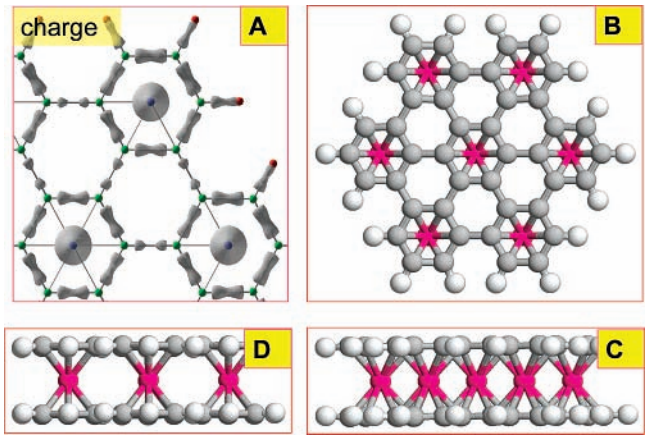

Figure 6. Electronic structure and geometry of the $Cr_7(C_{42}H_{18})_2$ sandwich. Panel A is a quadrant of the total charge density isosurface ($d_{iso} = 17\,500$, $d_{max} = 35\,641$). The rings containing a metal atom have fairly uniform C−C bond charge density. The inter-ring C−C bonds have a much lower charge density. The panels B, C, and D show the sandwich to be flat and uniform in cross sections with no discernible curvatures and all metal atoms on ring centers.

shows the ELF isosurface for elf = 0.4910 viewed from the top. Each ring has the circular "string-of-pearls" configuration of V(C, C) basins linked together on the metal side by six V(Cr, C, C) basins, analogous to those seen in the ELF of $Cr_1(C_6H_6)_2$.[32]

5. Results for Dibenzopyrene Sandwich $Cr_4(C_{24}H_{14})_2$

The ground state is a spin-paired singlet $S = 0$; a search for a spin-polarized, antiferromagnetic $S = 0$ ground state was not successful. The total DFT energy was found to be $E_{tot}[Cr_4(C_{24}H_{14})_2] = -571.397$ eV, and the DFT energy of the hydrocarbon moiety was $E_{tot}(C_{24}H_{14}) = -269.438$ eV, which gives a formation energy $\Delta E_f = 10.741$ eV, or 2.69 eV per chromium atom.

Figure 5A and B show the sandwich in top (⊥N) and side (⊥M) view; specific details of the geometry are given in Table 1. The metal sites are all similar, with the metal−ring gaps almost the same as in $Cr_1(C_6H_6)_2$. Figure 5C shows an isometric surface for the total charge ($d_{iso} = 14\,500/d_{max} = 28\,339$.). The total charge density of an isolated dibenzopyrene looks very similar to the hydrocarbon charge displayed in Figure 5C. All the C−C bonds connecting the rings contain less charge than the intraring bonds of the benzoidal centers, which is consistent with the notion of virtually independent benzoidal centers in both the hydrocarbon and the sandwich. Around each metal, the ELF has all the features displayed in Figures 2 and 3 except for small changes due to the local symmetry of the metal sites.

Figure 5C shows two isometric surfaces for total electronic charge. The left shows the merging of metal and hydrocarbon charge envelopes at low charge (~10%) density ($d_{iso} = 3000/d_{max} = 38\,339$). On the right, we show the isosurface at $d_{iso} = 14\,500$ (~50%), showing the density at which there is virtually no isosurface on the ring connector bonds between the benzenoid centers. The low density isosurface shows that the metal atoms merge in a partial circle corresponding to a buildup toward a η^6-coordinated ligand. This system exemplifies the 18e rule extended to four independent benzenoid centers.

6. Results for the Hexabenzocoronene Sandwich $Cr_7(C_{42}H_{18})_2$

The total DFT energy was calculated to be $E_{tot}[Cr_7(C_{42}H_{18})_2] = -953.085$ eV, and the DFT energy of the hydrocarbon moiety $C_{42}H_{18}$ was $E_{tot}(C_{42}H_{18}) = -449.060$ eV, which gives a formation energy $\Delta E_f = 16.850$ eV, or 2.40 eV per chromium atom. Given that the HOMO−LUMO gap BG_0 is 0.310 eV, the stability of the sandwich is not as high as for chromium bis-benzene ($\Delta E_f = 3.226$ eV, $BG_0 = 1.954$ eV).

Figure 6 shows the electronic charge density (A) and the geometry of the $Cr_7(C_{42}H_{18})_2$ sandwich (B− D). Panel A shows a sample quadrant of the total charge density as an isosurface ($d_{iso} = 17\,500/d_{max} = 35\,641$). Note that rings containing Cr atoms show fairly uniform charge in all six C−C bonds, whereas all the C−C bonds connecting the rings show much less charge. Table 1 showed these ring connecting bonds to be longer than the benzenoidal ring C−C bonds. There was a small difference in whether these C−C ring connecting bonds were oriented radially or circumferencially. Panel 6B shows the plan view structure with all metal atoms located between ring centers. In panels 4C and 4D, the side views of the sandwich structure show the cross sections to be even, so the sandwich appears to be flat with no curvature. Clearly, this large sandwich complies with the 18e rule extended to seven independent benzenoid centers.

Further confirmation comes from the geometric data listed in Table 1. In many important ways, the properties of the large structure parallel the small one, including Cr−ring gaps, C−C bonds, M−C bonds, <C−M−C bond angles, and C−C′ and H−H′ distances.

The ELF of the hexabenzocoronene sandwich showed all the general features reported for $Cr_1(C_6H_6)_2$, with a few small differences due to symmetry, bond lengths, and ring gaps. Figure 7A is a plan schematic showing the site symmetry of the central metal and two of the outer metal atoms. Figure 7B shows an orthographic plot of the ELF isosurface (elf = 0.14) viewed at a small angle to a plane through all the metal atoms (Cr atoms in blue). The view, between the two hydrocarbon valence basins, shows the metal atoms and their associated valence basins. The color of the plane is the ELF value (blue and light blue). The hydrocarbon C−C bond skeleton is also shown (C atoms green, top and bottom in the Figure). On the plane, three Cr atoms are visible, one on the central D_{6h} site (middle) and two on outer C_{2v} sites. Each metal site is surrounded by a hexagonal array of small-sized V(C, Cr, C) basins.

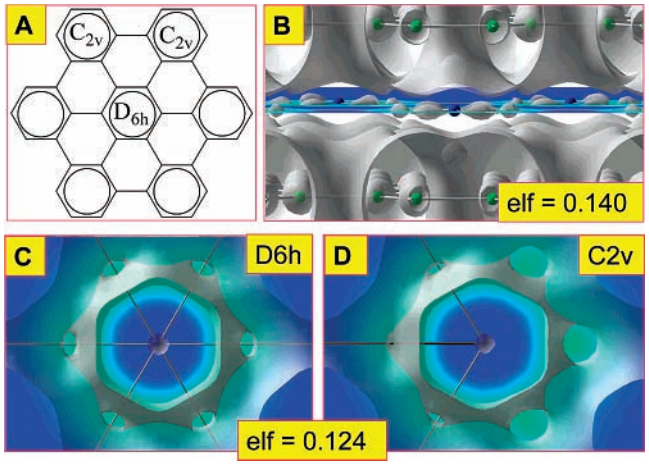

Figure 7. ELF of the sandwich $Cr_7(C_{42}H_{18})_2$ showing the region around the central metal atom. Panel A shows a hydrocarbon with three labeled metal sites. Panel B shows for the three metal sites the ELF isosurface (elf = 0.140) with the hydrocarbon valence basins above and below. Each metal atom (blue) is surrounded in the plane by the six V(C, Cr, C) basins that have not yet merged with the hydrocarbon basin. Panel C shows the ELF at elf = 0.124 for the central site with D_{6h} symmetry viewed along the *z*-axis. Panel D shows the same isosurface at a C_{2v} metal site. The chromium atoms are shown connected. The C_{2v} site has more strongly merged with the envelope of the hydrocarbon.

TABLE 3: $Cr_7(C_{42}H_{18})_2$ Energy (eV), Charge, Spin Density Vs Cr−Ring Separation (pm)

spin *S*	E_{tot} (−eV)	Cr−ring pm (min/max)	Cr1 (chg[a]/spin)	Cr2 (chg[a]/spin)	Cr4 (chg[a]/spin)
12	942.9	212/−	−/−	−/−	−/−
10	948.1	185/199	4.41/2.95	4.44/2.78	4.46/2.66
8	948.9	179/189	−/−	−/−	−/−
6	950.6	167/186	−/−	−/−	−/−
5	950.9	165/186	4.43/3.54	4.64/1.02	4.64/1.05
0	953.1	162/162	3.73/0.00	3.72/0.00	3.72/0.00

[a] chg = charge.

The central atom has in addition two nonbonding V(Cr) basins hidden but still faintly visible on the perpendicular *z*-axis behind the V(C, C) surfaces. Figure 7C shows a closeup of the central metal (elf = 0.124), surrounded by six linked basins with openings due to the merging with V(Cr, C, C). This is the analogue of Figure 3B, except we show wire connectors to the six surrounding metal atoms and not to carbon atoms. Figure 7D shows a C_{2v} site on an outer ring. The wire bonds link to three chromium atoms. The side of the C_{2v} site that has C atoms with attached H atoms has more strongly merged with the V(Cr, C, C) envelope of the hydrocarbon. This effect is due in part to differences in M−C and C−C bond lengths.

We close this section with a comment on the dependence of structure DFT total energy and spin vs gap between the hydrocarbons. Table 3 shows how the energy and spin changed during the course of a D_{2h} constrained dynamics geometry optimization. We give the maximum and minimum metal−ring separations as half the C−C′ separations. Atom Cr1 is centra,l and Cr2 and Cr4 are the two distinct D_{2h} atoms on 2-fold rotation axes. In the converged state, there was essentially no difference between Cr2 and Cr4. We note that the total spin, *S*, decreases monotonically along with the energy as the central Cr−ring gap decreases. Likewise, the spin density on the atoms decreases to zero and the charge density decreases to 3.73 for the central metal atom and slightly less for the perimeter metals. This Table shows there is a great sensitivity in the spin with gap, which explains in part why other structures can adopt antiferromagnetic spin configurations or high-spin configurations when other effects prevent the gap from closing.

TABLE 4: Geometry (Distances/pm; Angles/deg) for the Triphenylene Sandwich $Cr_3(C_{18}H_{12})_2$

Cr−Cr distances: Cr1−Cr2 = 513; Cr2−Cr2′ = 458
C−C distances between rings: ring 1−ring 2 = 142; ring 2−ring 2′ = 145

Cr1 site/C_{2v} symmetry/charge 5.17/spin 3.20
Cr1 site has two symmetry related C atoms near the metal atom

Cr1−ring	M−C	C−C	C−C′[a]	H−H′	∠C1−M−C2
202	218	142	403	435	37.97

Cr2 site/C_{σ} symmetry/charge 5.68/spin −1.56
Cr2 sites have four C atoms near the metal atom

Cr−ring[b]	M−C	C−C	C−C′	H−H′	∠C1−M−C2
Av(4) 166	Av(4) 215	Av(6) 226	Av(4) 332	Av(4) 322	Av(3) 29.4

[a] Ring of the Cr1 site is tilted outward; the three C−C′ distances are 403, 370, and 374 pm; table values are for the closest C−C bond. [b] Abbreviations: Av(*m*) = average of *m* values; C and C′ are eclipsed pairs of carbon atoms on opposing hydrocarbons.

7. Results for the Triphenylene Sandwich $Cr_3(C_{18}H_{12})_2$

The ground state was found to be a spin-polarized, antiferromagnetic, singlet $S = 0$ state with the axial metal atom carrying twice the spin of the second metal type. The isolated triphenylene molecule converged to a spin-paired D_{3h} symmetric ground state with a large HOMO−LUMO gap $BG_0 = 3.547$ eV. For the sandwich (starting from a D_{3h} initial geometry), a stable spin-paired singlet state could not be found. Instead, an antiferromagnetic state with C_{2v} symmetry was located. This we attribute to Jahn−Teller splitting of degeneracy arising from *d*-functions on the metal atoms. The antiferromagnetic sandwich did not resemble the $n = 1$, $n = 2$, $n = 4$, and $n = 7$ sandwiches reported above.

First, we briefly describe the geometry and electronic structure and then discuss why this fully benzenoid hydrocarbon did not yield a sandwich subject to the extended 18e rule. The main details of the geometry are summarized in Table 4. The total DFT energy of the triphenylene structure was $E_{tot} = -437.094$ eV. The energy of formation was $\Delta E_f = 6.149$ eV, or 2.05 eV/Cr atom; the HOMO−LUMO gaps for the separate spin manifolds were 0.742 eV and 0.168 eV for spin 1 (up) and spin 2 (down), respectively.

In Figure 8, panels A and B show the plan and side view of the ground electronic state. The sandwich was found to have distorted to C_{2v} from a D_{2h} starting geometry. The metal on the configuration axis was attached to a C−C bond pair in a C_{2v} symmetry site with a large metal−ring gap (range 196−204pm). The others are more centrally located in their assigned rings with metal−ring gaps (av 173 pm) significantly larger than the 162 pm in chromium bis-benzene but still much less than the Cr1 site (see Figure 8B). From the discussion in the last section concerning spin vs metal−ring gap (Table 3), we see this geometry as predisposed to high spin on Cr1 and two counter balancing low spins on Cr2 and Cr2′.

The total spin of the sandwich was zero. The spin on atom Cr1 was counter by the sum of spins on atoms Cr2 and Cr2′. In Figure 8D, the computed spin density (spin 2) is represented as an isosurface ($d_{iso} = -1000$) for the off-axis metal atoms (Cr2, Cr2′). The dotted circle around atom Cr1 depicts the isosurface for spin 1 (at value $d_{iso} = 1000$) for the opposite spin 1 density, which was localized exclusively on metal Cr1. The range of chromium atom spin density was from $d_{min} = -9131$ to $d_{max} = 17862$. Examination of how the spins were partitioned among atoms and orbitals provided little additional insight, except what might be expected. The C_{2v} symmetry site Cr1 had less mixing than the lower symmetry sites occupied by Cr2 and Cr2′.

Figure 8C provided significant evidence regarding the lack of isolation of the aromatic rings. In panel 8C, the left side

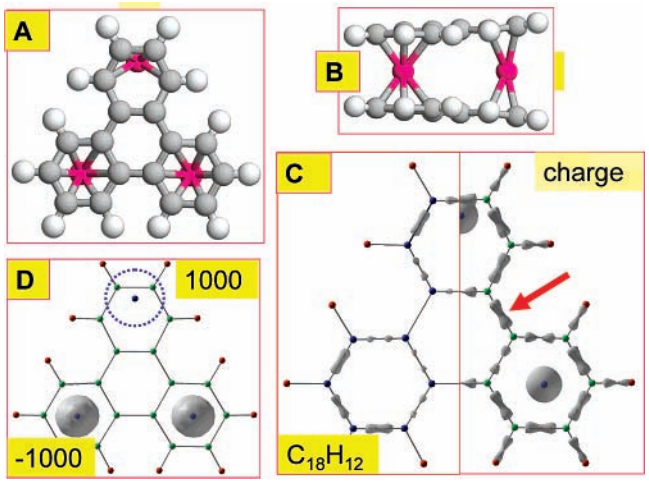

Figure 8. Geometry, electronic structure, and antiferromagnetic spin density for the triphenylene sandwich $Cr_3(C_{18}H_{12})_2$. Panels A and B show that the geometry of the sandwich is highly distorted from planarity. The C_{2v} site metal has the highest spin (large gap). Panel C, left side, shows the charge on the isolated triphenylene (d_{iso} = 12,-500/d_{max} = 13,480). Note the weak charge on the ring connecting bonds and the nonuniform charge in the rings. Panel C, right side, shows the charge in the sandwich. The arrow points to the strong inter-ring charge. Figure D shows the spin density on the C_{2v} metal atom (spin 1, d_{iso} = 1000, dotted blue circle) and the spin on the two C_σ sites (spin 2, d_{iso} = −1000).

labeled $C_{18}H_{12}$ shows the total charge density (d_{iso}= 12 500/d_{max}= 13 480) in the isolated molecule. Whereas this isosurface shows the absence of charge in the three ring connector C−C bonds, it also shows a strong polarization away from uniformity among the intraring C−C bonds, contrary to the conclusion based on the simple VB theory. The additional VB diagram with double bonds connecting the rings does not describe the observed physics, even though it would reinforce a *cis*-butadiene π-structure in the rings. The calculated molecule charge suggests that metal atoms in the sandwich will not be centrally located in the rings. This is what Figure 8A and 8B show. Furthermore, the calculated charge density of the sandwich, shown on the right-hand side of Figure 8C has a significant charge on the connector C−C bond, as indicated by the arrow. This isosurface (d_{iso} = 11 550/d_{max} = 23 332) also shows that as in the isolated molecule, no C_6 ring has uniform charge, signifying benzenoid character. In summary, the failure of this system to form an 18e-rule-compliant structure could be attributed to nonbenzenoid charge distribution in the hydrocarbon rings, which promoted the migration of metal atoms off the ring center positions, and high initial symmetry, permitting a Jahn−Teller splitting among the metal−ring interactions.

8. Results for Coronene Sandwich $Cr_3(C_{24}H_{12})_2$

Like the triphenylene sandwich, this system was not found to be not 18e-rule-compliant. This system was originally included to test robustness of the 18e rule, the notion being that there were more than enough electrons and rings to go around.

The total DFT energy of the $Cr_3(C_{24}H_{18})_2$ sandwich was E_{tot} = −546.915 eV, the HOMO−LUMO gaps for the two spin manifolds were BG_1 = 0.219 eV (spin 1 (up)), and BG_2 = 0.639 eV (spin 2 (down)). The ground state was an antiferromagnetic singlet S = 0. The DFT energy data calculated for an isolated coronene molecule was $E_{tot}(C_{24}H_{12})$ = −262.980 eV (singlet S = 0, BG_0 = 2.869 eV; the triplet S = 1 state is calculated to lie 2.471 eV higher). The formation energy from eq 4 for $Cr_3(C_{24}H_{12})_2$ is ΔE_f = 4.62 eV. This is clearly not enough for a robust structure. During the course of the calculation, the sandwich geometry first settled into a high spin S = 6 state

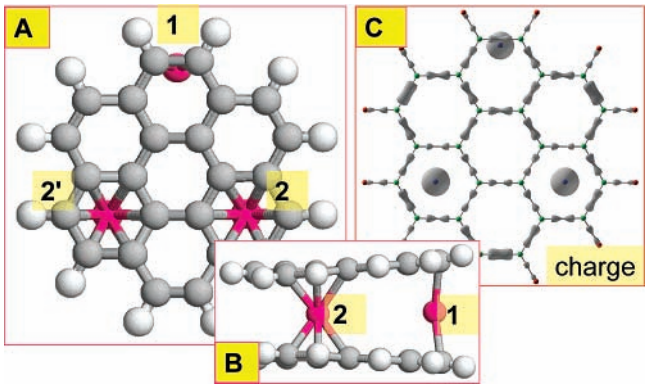

Figure 9. Geometry and electronic structure of the antiferromagnetic coronene sandwich $Cr_3(C_{24}H_{18})_2$. Panels A and B shows the geometry that resembles the triphenylene sandwich (see Figure 8). Panel C shows the charge density (d_{iso} = 11 700, d_{max} = 23 437). No ring has uniform charge.

TABLE 5: Geometry (Distances/pm; Angles/deg) for the Coronene Sandwich $Cr_3(C_{24}H_{18})_2$

Cr−Cr distances: Cr1−Cr2 = 521; Cr2−Cr2′ = 446

Cr1 site/C_{2v} symmetry/charge 5.14/spin −3.48
Cr1 site has two symmetry related C atoms near the metal atom

Cr1−ring[a]	M−C	C−C	C−C′*	∠C1−M−C2
204	216	143	407	38.4

Cr2 site/C_σ symmetry/ charge 5.57/spin +1.76
Cr2 sites have four C atoms near the metal atom

Cr−ring[a]	M−C	C−C	C−C′	∠C1−M−C2
Av(6) 173[b]	Av(6) 231	Av(3) 142	Av(6) 345	Av(3) 38.0

[a] M−ring = $^1/_2$(C−C′). [b] Range 161−179 pm; Av(m) = average of m values; C−C′ (H−H′) are eclipsed pairs of C (H) atoms; "/" separates values of symmetry distinct sites.

with energy E_{tot} = −545.971 eV. It was only by looking for an antiferromagnetic final state that we identified the ground state described above.

Figure 9A and 9B show results for the geometry and the total charge. There is an obvious similarity in overall appearance to the triphenylene sandwich shown in Figure 8. One metal atom sits on a C_{2v} axis site between perimeter C−C bonds, and the other two metal atoms occupy close to initially assigned ring center positions. Table 5 provides more details of the geometry. Because the C_{2v}-axis site has a large metal−ring spacing, the Cr1 spin was high. In fact, the calculated spin distribution is qualitatively similar to the triphenylene structure, with the high-spin density on the C_{2v} metal atom balancing twice the smaller spin distribution on the two C_σ, which with somewhat smaller gaps have a lower spin sites. Figure 9C shows an isometric surface of the total charge density (d_{iso}= 11 700; d_{max} = 23 437), in which the three most prominent C−C bonds are the double bonds (C−C = 137 pm) depicted on the coronene structure in Figure 1. The two rings with central metal atoms do not have uniformly distributed charge. The rings with metal atoms do not appear to be independent of each other.

Examination of the charge density in an isolated $C_{24}H_{18}$ molecule showed that there was a fair uniformity in all interior C−C bonds. On the perimeter, the picture was quite different. The largest charge occurred on the six symmetrically distributed −(H)C−C(H)− bonds with H atoms. In other words, the distribution appears as if there were a C═C double bond between each adjacent pair of C(H) atoms with an H atom attached. The corresponding VB diagram has six radially directed C═C double bonds. Accordingly, the aromaticity of coronene, which provides the molecule with its stability (large

HOMO−LUMO gap), does not also provide the independent benzenoidal centers, which are necessary for a rule to predict chromium sandwiches.

The main reasons why the coronene sandwich did not follow the 18e rule are the same as for the triphenylene sandwich. In the isolated molecule, contrary to a simple VB argument, there were no independent benzenoid structures, and the charge along the perimeter corresponded to six symmetrically disposed C═C double bonds. The trigonal D_{3h} initial symmetry, with degenerate metal *d* functions, caused the system to undergo Jahn−Teller distortion to C_{2v} symmetry. A detailed analysis of this effect is not within the scope of this report.

9. Summary and Discussion

This paper studied the electronic and geometry structure of a series of sandwich structures containing chromium atoms as the central layer using a modern ab initio quantum electronic structure method. The largest sandwich, $Cr_7(C_{42}H_{18})_2$, which consisted of seven chromium atoms between two *s*-hexabenzocoronenes, had properties remarkably similar to chromium bis-benzene, $Cr_1(C_6H_6)_2$, the smallest member of the series and a known molecule. The series tested the idea that the 18e rule could be extended to hydrocarbons consisting of "independent" aromatic centers. For those systems for which the idea worked (benzene, biphenyl, dibenzopyrene, hexabenzocoronene), we found that the ELF provided insight into the chemical bonding around the chromium centers. For example, the nonbonding ELF basin for the spin-paired d_{z2}-function electrons.

For the sandwiches with triphenylene, $Cr_3(C_{18}H_{12})_2$, and coronene, $Cr_3(C_{24}H_{12})_2$, the rule did not work. The breakdown was attributed to (1) an absence of well-defined benzenoid C_6 centers in the molecules and (2) symmetry breaking.

Simple VB notions did not describe triphenylene well enough, and the DFT calculations showed valence charge polarization toward the extremity of the rings, creating a favored metal site further from the center of the molecule. This repositioning has been noted in other transition metal sandwich structures wherein there was no opportunity for the 18e rule to work.[1−4] That the rule did not work for coronene was not a surprise, since it did not satisfy the criteria as well as triphenylene. The relaxation of symmetry from D_{3h} to C_{2v} in both $Cr_3(C_{18}H_{12})_2$ and $Cr_3(C_{24}H_{12})_2$ provided the second process to be avoided for the 18e rule to be useful in predicting sandwich structures. In these 3-fold symmetric systems, the metal *d* functions can combine into degenerate levels that are split apart by the Jahn−Teller effect. A detailed study of this effect for the structures under consideration here is not within the scope of this report. The symmetry relaxation and a larger metal−ring gap created the right conditions for the formation of the singlet antiferromagnetic spin state.

Finally, we comment that this work touches on issues in the design of graphene structures.[38−39] A simple example would be the "welding" of crossed strips using transition metals. Another of potential interest is the control of conductivity in nanowide strips using crenellated edges. The importance of design with embedded fully benzenoid hydrocarbon structures has yet to be exploited.

Acknowledgment. M.R.P. thanks the Center for Computational Materials Science for warm hospitality and financial support. All calculations were performed on the Supercomputer Facility at IMR, Tohoku University. The authors thank the staff of the Supercomputer Facility, Institute of Materials Research, Tohoku University, for their enthusiastic and dedicated support.

References and Notes

(1) Murahashi, T.; Fujimoto, M.; Oka, M.; Hashimoto, Y.; Uemura, T.; Tatsumi, Y.; Nakao, Y.; Ikeda, A.; Sakaki, S.; Kurosawa, H. Discrete sandwich compounds of monolayer palladium sheets. *Science* **2006**, *313*, 1104. This paper opened an avenue to transition metal sandwich compounds through the synthesis of two the molecular ions $[Pd_3Cl_3(C_7H_7)_2]^{2+}$ and $[Pd_5(C_{18}H_{12})_2\ C_6H_5CH_3]^{2-}$. The Pd_5 complex comprised a planar array of palladium with η^2- and η^3-coordination of the metal atoms to edge carbon atoms of the tetracene ($C_{18}H_{12}$) moieties. The authors performed DFT calculations using the hybrid B3LYP functional.

(2) Philpott, M. R.; Kawazoe, Y. *Mater. Trans.* (*Japan*) **2007**, *48*, 689.

(3) Philpott, M. R.; Kawazoe, Y. *Chem. Phys.* **2007**, *337*, 55.

(4) Philpott, M. R.; Kawazoe, Y. *Chem. Phys.***2007**, *342*, 223.

(5) Clar, E. *Polycyclic Hydrocarbons;* Academic Press: London, 1964; Vol. 1, Chapter 6, p 32.

(6) For references to the 18e rule, see: Orgel, L. S. *An Introduction to Transition Metal Chemistry Ligand Field Theory;* Methuen: London, 1961; Chapter 10. Cotton, F. A.; Wilkinson, G.; Murillo, C. A.; Bochmann, M. *Advanced Inorganic Chemistry*, 6th ed.; Wiley: New York, 1999. Mitchell, P. R.; Parish, J. The eighteen-electron rule. *J. Chem. Educ*. **1969**, *46*, 811.

(7) Armitt, T. W.; Robinson, R. J. *Chem. Soc*. **1925**, 1604.

(8) Clar, E. *Polycyclic Hydrocarbons*; Academic Press: London, 1964; Vols. 1 and 2.

(9) Hill, J. P.; Jin, W.; Kosaka, A.; Fukushima, T.; Ichihara, H.; Shimomura, T.; Ito, K.; Hashizume, T.; Ishii, N.; Aida, T. *Science* **2004**, *304*, 1481.

(10) Pyykko, P. *J. Organomet. Chem.* **2006**, *691*, 4336.

(11) . Suresh, C. H.; Gadre, S. R. *J. Org. Chem.* **1999**, *64*, 25.

(12) Kealy, T. J.; Pauson, P. L. *Nature* **1951**, *168*, 1039. Miller, S. A.; Tebboth, J. A.; Tremaine, J. F. *J. Chem. Soc*. **1952**, 632.

(13) Resa, E.; Carmona, E.; Gutierrez-Puebla, E.; Monge, A. *Science* **2004**, *305*, 1136.

(14) Xie, Y.; Schaefer, H. F., III; Jemmis, E. D. *Chem. Phys. Lett*. **2005**, *402*, 414.

(15) Philpott, M. R.; Kawazoe, Y. *Chem. Phys*. **2006**, *327*, 283.

(16) Philpott, M. R.; Kawazoe, Y. *J. Mol. Struct.: THEOCHEM* **2006**, *773*, 43.

(17) Philpott, M. R.; Kawazoe, Y. *J. Mol. Struct.: THEOCHEM* **2006**, *776*, 113.

(18) Haiduc, I. L. Y.; Goh, L. Y. *Coord. Chem. Rev*. **2002**, *224*, 151.

(19) Kresse, G.; Hafner, J. *Phys. Rev. B: Condens. Matter Mater. Phys.* **1993**, *47*, 588.

(20) Kresse, G.; Hafner, J. *Phys. Rev. B: Condens. Matter Mater. Phys.* **1994**, *49*, 14251.

(21) Kresse, G.; Furthmuller, F. *Comput. Mater. Sci*. **1996**, *6*, 15.

(22) Kresse, G.; Furthmuller, F. *Phys. Rev. B: Condens. Matter Mater. Phys.* **1996**, *54*, 11169.

(23) Blöchl, P. E. *Phys. Rev. B: Condens. Matter Mater. Phys.* **1994**, *50*, 17953.

(24) Kresse, G.; Joubert, J. *Phys. Rev. B: Condens. Matter Mater. Phys.* **1999**, *59*, 1758.

(25) Perdew, J. P. Unified theory of exchange and correlation beyond the local density approximation. In *Electronic Structure of Solids 1991*; Ziesche, P., Eschrig, H.; Akademie-Verlag: Berlin, 1991.

(26) Perdew, J. P.; Chevary, J. A.; Vosko, S. H.; Jackson, K. A.; Pederson, M. R.; Singh, D. J.; Fiolhais, C. *Phys. Rev. B: Condens. Matter Mater. Phys.* **1992**, *46*, 6671.

(27) de P. R. Moreira, I.; Costa, R.; Filatov, M.; Illas, F. *J. Chem. Theo. Chem.* **2007**, *3*, 764.

(28) Illas, F.; de P. R. Moreira, I.; Bofil, J. P.; Filatov, M. *Phys. Chem. Chem. Phys.* **2006**, *8*, 645.

(29) Becke, A. D.; Edgcombe, K. E., *J. Chem. Phys*. **1990**, *92*, 5397.

(30) Silvi, B.; Savin, A. *Nature* **1995**, *371*, 683.

(31) Grützmacher, H. T. F.; Fässler, T. F. *Chem.—Eur. J*. **2000**, *6*, 2317.

(32) Frison, G.; Servin, A. *Internet Electron. J. Mol. Des.* **2004**, *3*, 222.

(33) Vaspview data viewer (http://vaspview.sourceforge.net); RASMOL structure viewer (http://www.umass.edu/microbio/rasmol/).

(34) Haaland, A. *Acta Chem. Scand.* **1965**, *19*, 41.

(35) Haaland, A. *Acc. Chem. Res*. **1979**, *12*, 415.

(36) Philpott, M. R.; Kawazoe, Y. Unpublished calculations on organometallic and transition metal sulphide molecules, 2007.

(37) Rayon, V. M.; Fenking, G. *Organometallics* **2003**, *22*, 3304.

(38) Novoselov, K. S.; Jiang, D.; Schedlin, F.; Khotkevich, V. V.; Morozov, S. V.; Geim, A. K. *Proc. Nat. Acad. Sci. U.S.A.* **2005**, *102*, 10451.

(39) Geim, A. K.; MacDonald, A. H. Graphene: Exploring Carbon Flatland. *Phys. Today* **2007**, *60* (8), 35.